Fuel Cell Research at the University of Delaware

Final Report

Jingguang G. Chen, Professor of Chemical Engineering
Suresh G. Advani, Professor of Mechanical Engineering

Introduction

The grant initiated nine basic and applied research projects to improve fundamental understanding and performance of the proton exchange membrane (PEM) fuel cells, to explore innovative methods for hydrogen production and storage, and to address the critical issues and barriers to commercialization. The focus was on catalysis, hydrogen production and storage, membrane durability and flow modeling and characterization of Gas Diffusion Media. Three different types of equipment were purchase with this grant to provide testing and characterization infrastructure for fuel cell research and to provide undergraduate and graduate students with the opportunity to study fuel cell membrane design and operation. They are (i) Arbin Hydrogen cell testing station, (ii) MTS Alliance™ RT/5 material testing system with an ESPEC custom-designed environmental chamber for membrane Durability Testing and (iii) Chemisorption for surface area measurements of electrocatalysts. The research team included ten faculty members who addressed various issues that pertain to Fuel Cells, Hydrogen Production and Storage, Fuel Cell transport mechanisms. Nine research tasks were conducted to address the critical issues and various barriers to commercialization of Fuel Cells. These research tasks are subdivided in the general areas of (i) Alternative electrocatalysis (ii) Fuel Processing and Hydrogen Storage and (iii) Modeling and Characterization of Membranes as applied to Fuel Cells research.. The summary of accomplishments and approaches for each of the tasks is presented below

I.CATALYSIS:

Task 1: Alternative Electrocatalysts for Hydrogen and Methanol Fuel Cells
PI: Jingguang Chen, Chemical Engineering

Task 2: Task 2: Rational Catalyst Design for the Preferential Oxidation of Carbon Monoxide
PIs: Jochen Lauterbach, Chemical Engineering

Task 3: CVD and ALD as Alternative Synthesis Techniques for Electrocatalysts
PIs: Robert Birkmire, Institute for Energy Conversion and Brian Willis, Chemical Engineering

II. HYDROGEN STORAGE AND FUEL PROCESSING :

One vision of the future of energy delivery is the "Hydrogen Economy." In this vision, hydrogen-powered fuel cells provide power for vehicles and for distributed fixed power sources. Key technological hurdles include hydrogen generation (especially without CO_2 generation), transportation and storage. The US Department of Energy has issued a "Grand Challenge" encompassing many basic research needs for the Hydrogen Economy, and has also set performance milestones for future hydrogen storage technologies.

Task 4: Identification and Investigation of Novel Materials for Hydrogen Storage
PI: Andrew Goudy, Delaware State University

Objective: Determine the Hydriding Behavior of Selected Alanate Materials.by conducting the following subtasks:

a) Determine the x-ray diffraction peak pattern of each alanate material as well as mixtures of alanates and make comparisons.
b) Mix the various alanate materials with a catalyst using a SPEX Mill.
c) Run thermal gravimetric analyses (TGA) on the catalyzed alanate materials and mixtures of them.
d) Perform PCI measurements on selected alanates.

Approach:

Lithium alanate and sodium alanate samples as well as titanium (III) chloride catalyst were obtained from the Aldrich Chemical Co. X-ray powder diffraction analyses were determined on the samples using a Panalytical X'Pert Pro MPD Analytical X-Ray Diffractometer Model PW3040 Pro. Analyses were done using copper K-alpha radiation. Prior to thermal analysis, samples were mixed with 4 mole percent titanium chloride using a SPEX 8000M Mixer/Mill. All samples were handled in a Vacuum/Atmospheres argon filled glove box to protect them from exposure to air and moisture. The glove box was capable of achieving less than 1% oxygen and moisture. TGA analyses were done on a Lab System – Diamond TG/DTA. Scans were run under an argon atmosphere by allowing 99.999% pure argon to flow through the system. The temperature was increased at 5 degrees per minute.

PCI analyses were done on a Sievert's apparatus. This manual apparatus consisted of a stainless steel manifold with ports for adding hydrogen evacuating, and venting. Ashcroft gauges were used for measuring pressures up to 3000 psi. A tube furnace was used to keep the sample at constant temperatures to within $\pm 0.5\ ^{o}C$. A mass flow meter (MKS) with a range of 0 to 1 standard 1 H_2 min was capable of measuring hydrogen flows to or from the sample reactor. Pressure-composition isotherms for hydrogen desorption from a sample were determined by allowing a known quantity of hydrogen to flow from a fully charged sample out through water into an inverted burette to atmospheric pressure. After waiting a sufficient period of time for equilibrium, the pressure was recorded and the process repeated until the sample was depleted of hydrogen. Absorption isotherms were obtained by first evacuating all of the hydrogen from the sample and sealing off the reactor chamber.

A calibrated volume was then charged with hydrogen and the pressure was recorded. The sample chamber was then reopened and after the absorption process was completed, the final pressure was recorded. The sample chamber was again closed, the calibrated volume was recharged, and the absorption process repeated until the sample was fully charged.

Results and Discussion

The materials studied in this research included sodium alanate, lithium alanate. We are currently examining various mixtures of these two materials. Figures 1 and 2 contain spectra for sodium alanate and lithium alanate respectively. There are significant differences in the spectra of these two materials and XRD can be used to differentiate the two materials and to determine phase purity. Mixtures of these two materials are expected to contain peaks from both spectra. However, if mechanical alloying has happened during mixing we should expect to see new peaks arising.

Sodium alanate, $NaAlH_4$, contains 7.5% hydrogen and lithium alanate, $LiAlH_4$, contains 10.5% hydrogen. Both of these materials are of interest because their hydrogen holding capacities exceed the year 2010 capacity of 6% established by DOE. Unlike interstitial intermetallic hydrides, these compounds generally release hydrogen through a series of decomposition reactions. Sodium alanate, for example, releases hydrogen in two consecutive steps shown below.

$$3\ NaAlH_4 \rightarrow Na_3AlH_6 + 2\ Al + 3\ H_2$$

$$Na_3AlH_6 \rightarrow 3\ NaH + Al + 3/2\ H_2$$

In the reactions shown above for sodium alanate, 3.7% by weight of the hydrogen is released in the first step and 1.9% is released in the second step, for a total of 5.6 wt. %. The hydrogen that is part of NaH is strongly bound to Na and is not released under normal reaction conditions. However, in order to be useful for hydrogen storage, a hydride must absorb and release hydrogen in a reasonable temperature interval. Therefore thermal gravimetric analyses, TGA, were done on each material and their mixtures to determine at what temperature hydrogen is released. The TGA graphs for sodium alanate, lithium alanate are shown in Figures 3 and 4 respectively. The graphs show that the desorption temperature of sodium alanate is higher than that of lithium alanate. This indicates that $NaAlH_4$ is a more stable hydride than $LiAlH_4$. Both materials release approximately 4% of the hydrogen in a moderate temperature interval. This corresponds to the first step in the two-step mechanism shown above. More hydrogen would have been released if the temperature had been taken to higher values. It should be noted that the graphs in Figures 3 and 4 display greater than 100 weight percent in the initial stages. This is believed to be caused by the samples picking up trace contaminants in the argon gas. In order to avoid this, plans are underway to run analyses in a TGA that is completely enclosed in an argon filled glove box. In addition, the amount and nature of the catalyst will be varied to determine what effect this has on the desorption temperature.

A PCI isotherm is currently being determined for $NaAlH_4$. Desorption and absorption curves have been determined at 200 ^oC. The curves show that, at this temperature, a phase transition occurs at approximately 32 atm. The fact that both desorption and absorption curves can be determined shows that the process is completely reversible. Isotherms will also be determined at two additional temperatures.

None of the research findings in the present study has been published. However, they will be presented at the October 2006 International Symposium on Metal Hydrogen Systems to be held in Hawaii, USA. The results will be submitted for publication shortly after the symposium. One Delaware State University graduate student is presently completing a Master's thesis on this research.

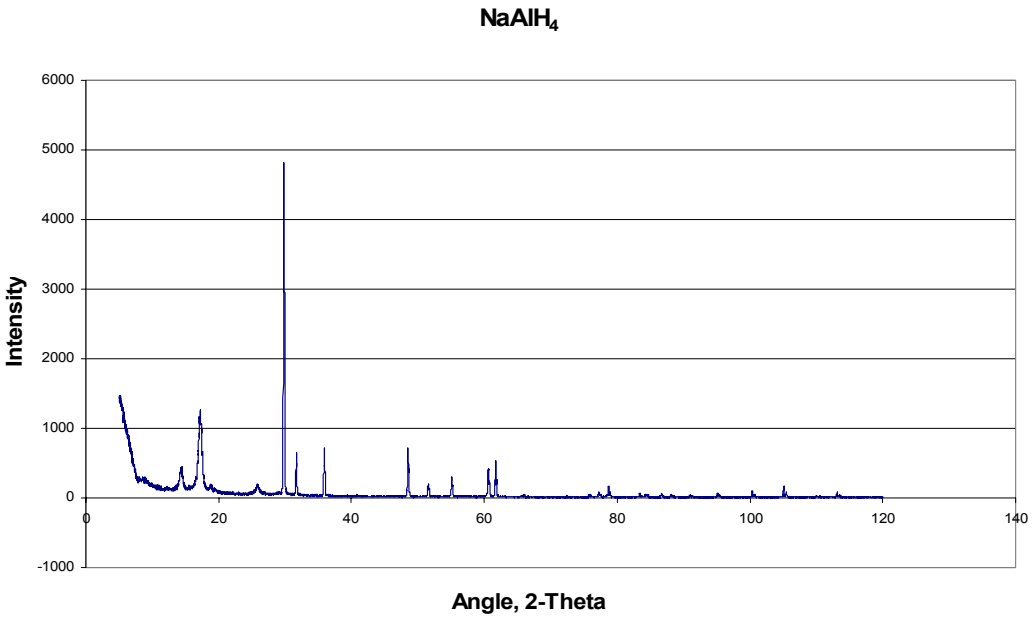

Figure 1. $NaAlH_4$ in Argon. The major peak occurs at 29.8 degrees. All of the major peaks occur before 62 degrees.

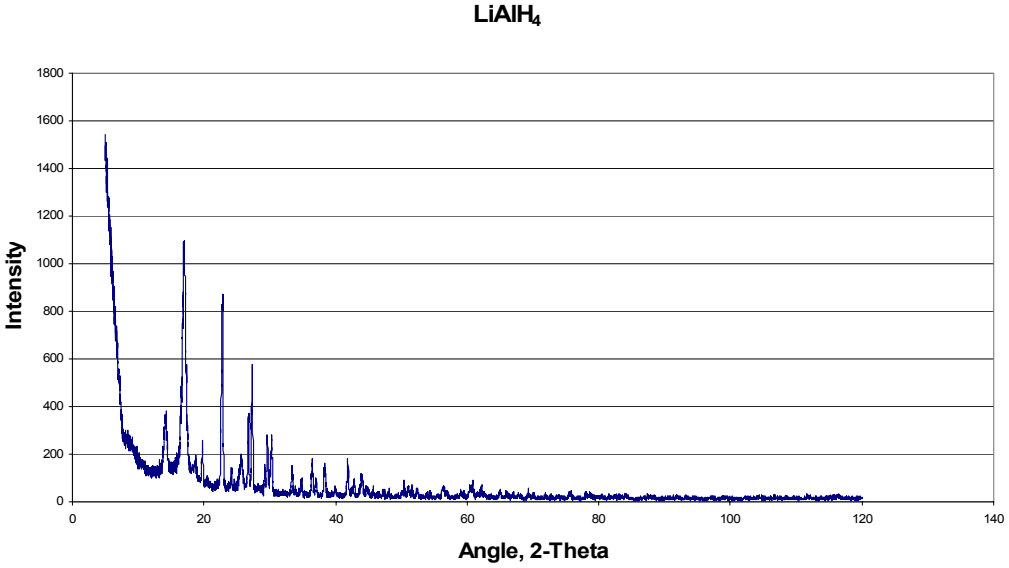

Figure 2. $LiAlH_4$ in Argon. The major peak occurs at 17 degrees. All of the major peaks occur before 45 degrees.

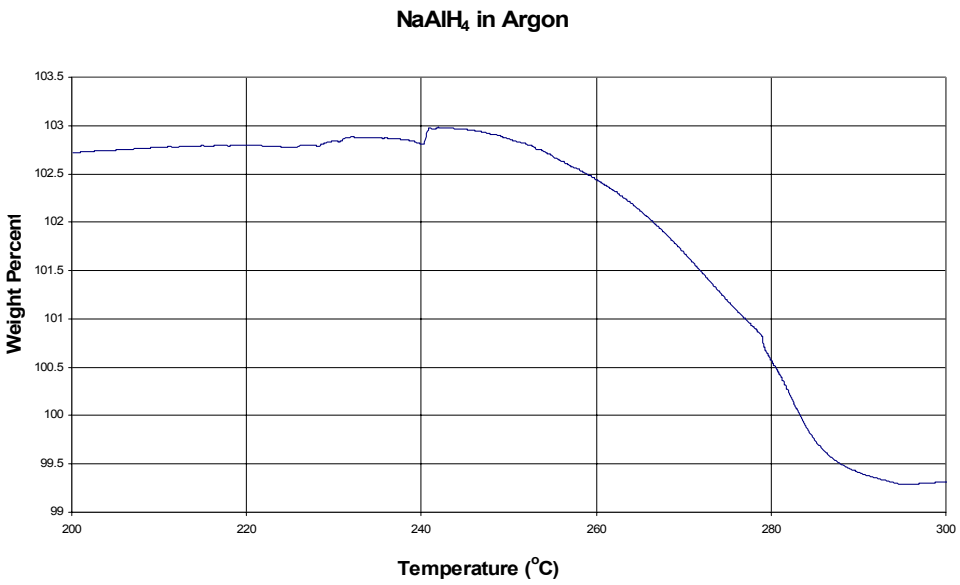

Figure 3. $NaAlH_4$ in Argon. Sample loses mass in the 240 - 295 °C temperature range. The total change in mass is approximately 4%.

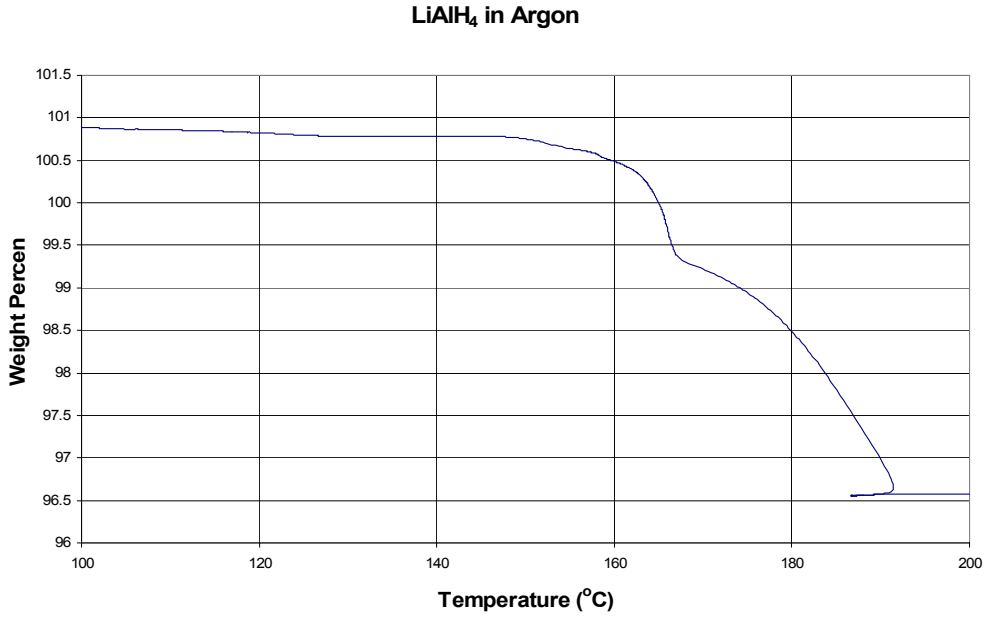

Figure 4. $LiAlH_4$ in Argon. Sample loses mass in the 150 - 190 °C temperature range. The total change in mass is approximately 4%.

Task 5: Fuel Cell Modeling & Hydrogen Reforming: Separation of Hydrogen from Gases using Carbon Nanotubes and Nanoporous Carbons
PI: Norman J. Wagner, Chemical Engineering

Task 6: Partial Oxidation at Short Contact Times as an Alternative Fuel Processing Route for Fuel Cells
PI: Dion Vlachos, Chemical Engineering

III. FLOW MODELING AND CHARACTERIZATION OF GDMs AND PEMs

The number one barrier to widespread use of Fuel Cells as identified by the Breakthrough Technologies Institute in a recent report was cost reduction and reliability improvements. To address this issue, one must understand and be able to characterize the transport mechanisms of the fluids in the Fuel Cell assembly and develop characterization methods to quantify the efficiency of operation and put forth life cycle predictive models.

Task 7: Permeability Characterization and Flow Visualization of Gas Diffusion Media Used in Fuel Cells
PIs: Suresh Advani and Ajay Prasad

Task 7: Permeability Characterization and Flow Visualization of Gas Diffusion Layer Used in Fuel Cells
PIs: Suresh Advani and Ajay Prasad

Introduction:

At the heart of a proton exchange membrane fuel cell (PEMFC) is a membrane electrode assembly (MEA), comprising a proton conducting membrane sandwiched between two catalyst containing electrodes. On top of the electrodes a porous gas diffusion layer (GDL) is placed to facilitate access of the Pt-containing catalyst to the fuel on the anode and the oxidant (usually air) on the cathode. The GDL must also transport away water (in vapor and/or liquid form) from the PEM. Currently there are few established standard methods to characterize the available GDLs and no published experimental techniques to visualize flow of fluids directly or indirectly inside such porous media. Knowledge of transport phenomena inside the architectures of such GDLs will lead to realistic models to describe the flow and will permit development of optimal designs of GDL pores to facilitate efficient transport of reactant gases and lead to highest efficiency, power output and energy density. GDL assemblies that can combine the optimal balance of porosity (to maximize the transport of gases and ions) and hydrophobicity gradient (to prevent water buildup on the cathode) are highly desirable.

Objectives:

Our goals were to (i) formulate and fabricate a characterization facility that will measure and calculate the local permeability of GDLs as a function of its pore size and distribution, (ii) determine the role of these GDL on fuel cell performance, (iii) examine

the role of convection in mass transport inside the cell to reduces losses and (iv) develop flow visualization techniques to understand the two phase transport inside the cell.

Approaches and Accomplishments

(i) Radial Permeability Characterization:

A radial permeability experiment was designed and fabricated to characterize and differentiate in-plane permeability of three gas diffusion layers manufactured by different techniques. The three different types of GDLs that were examined are shown in Figure 1.

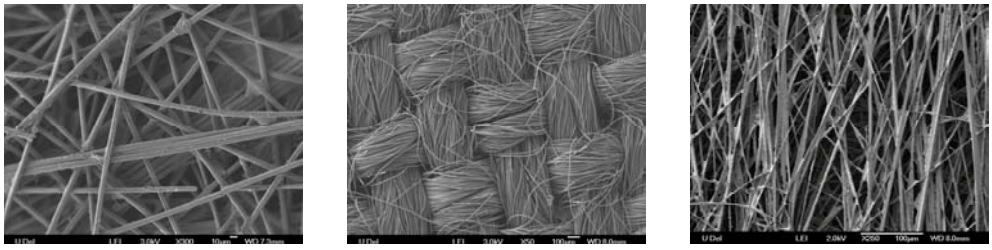

Figure 1: Permeability of three different types of GDLs was characterized (a) Carbon paper (b) carbon cloth and (c) SGL 31BA (non-woven material)

The schematic of the radial permeability set-up that was designed and fabricated is shown in Figure 2.

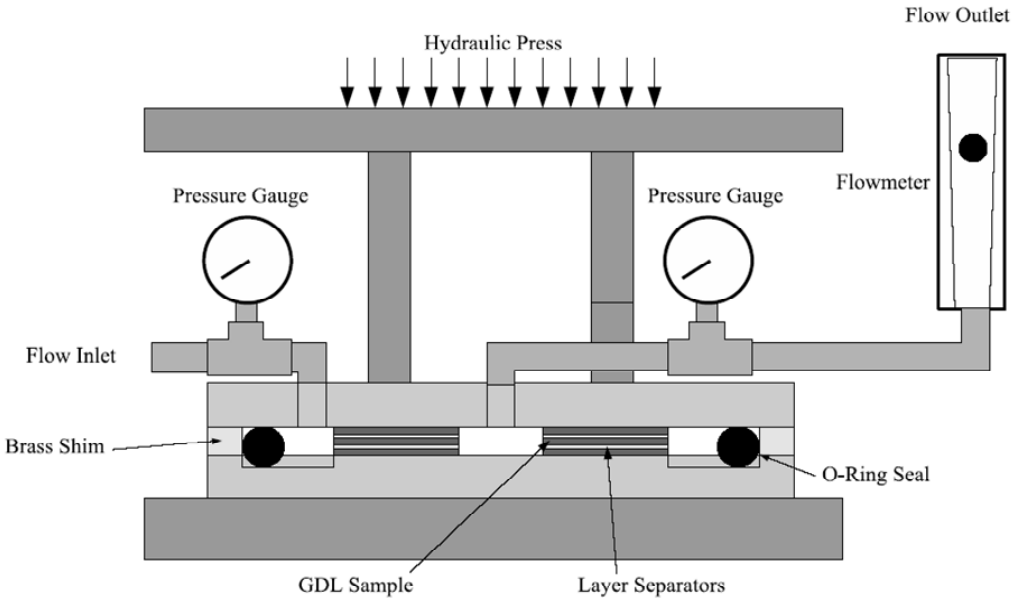

Figure 2: A radial characterization set-up to measure GDL in plane permeability

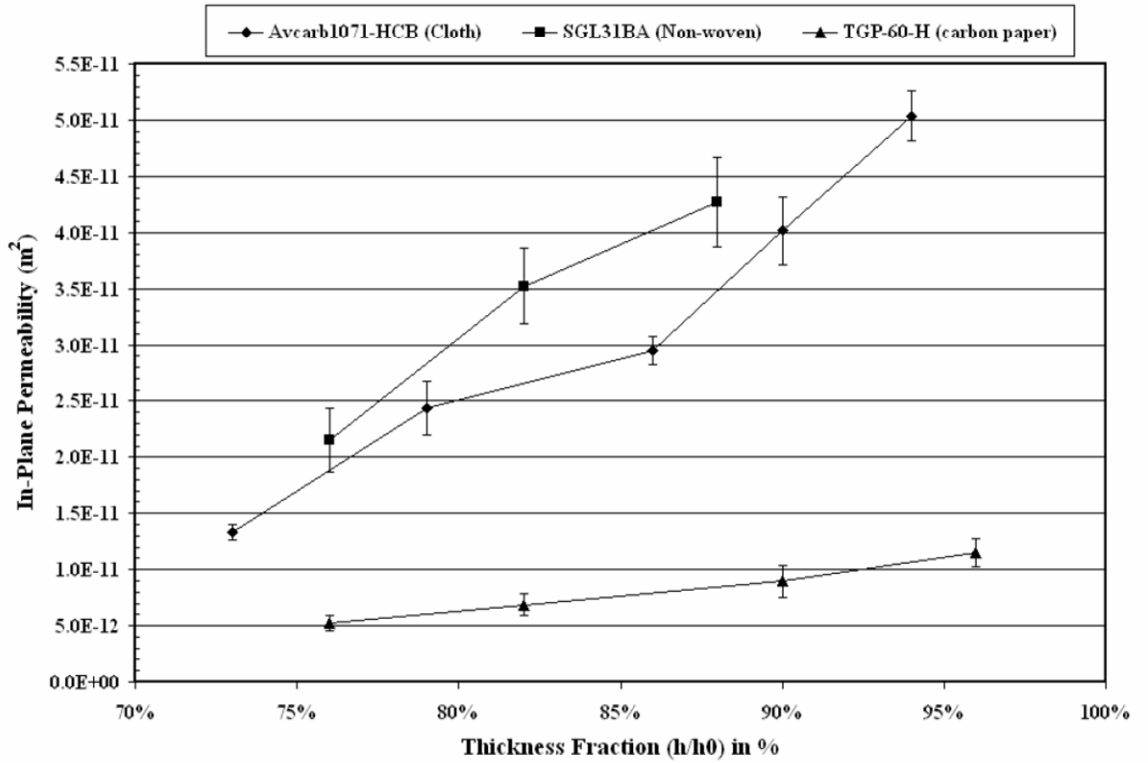

Figure 3: In-plane Permeability variation with compression of the GDL for the three types of GDL examined.

It was shown that experiments can use either a wetting liquid or a gas of known viscosity as the host fluid and reach identical conclusions. However, flowrates' dependence on pressure is different for gases and liquids and must be recognized when large pressure differentials are present.. A methodology was developed to address issues such as use of gas instead of liquid, sensitivity of the equipment and accurate measurement of small pressure drops. A pressure sensor in the form of a sheet can be used to characterize the pressure distribution under compressive loads and during transport to extract information about fluid flow as well. Table 1 shows the initial thicknesses used of these materials along with the compression ratios for which the permeability experiments were conducted.

Sample	Initial Thickness, h_o	Thickness Fractions (%), $h/h_o \times 100$
Avcarb 1071-HBC	335μm	94%, 90%, 86%, 79%, 73%
SGL31BA	318μm	88%, 82%, 76%
TGP-60-H	192μm	96%, 90%, 82%, 76%

Table 1: Compression ratios of various GDLs used

The results are shown in Figure 3.

(ii) Characterization of GDL performance in operational fuel cell

Humidification was carefully optimized in PEM fuel cells. Extremes in humidity levels at both the low end (membrane dehydration) and the high end (cathode flooding) of the

range can seriously reduce PEM Fuel Cell (PEMFC) performance. Due to the conflicting requirements for a PEMFC operation, the region of suitable operating conditions is very narrow. The cell is usually operated at the flooding limit, and some areas of the catalyst layer can easily become flooded by condensed water. Since flooding has been identified as one of the main current-limiting processes, understanding and optimizing liquid water transport throughout the cell is critical to improving PEMFC performance.

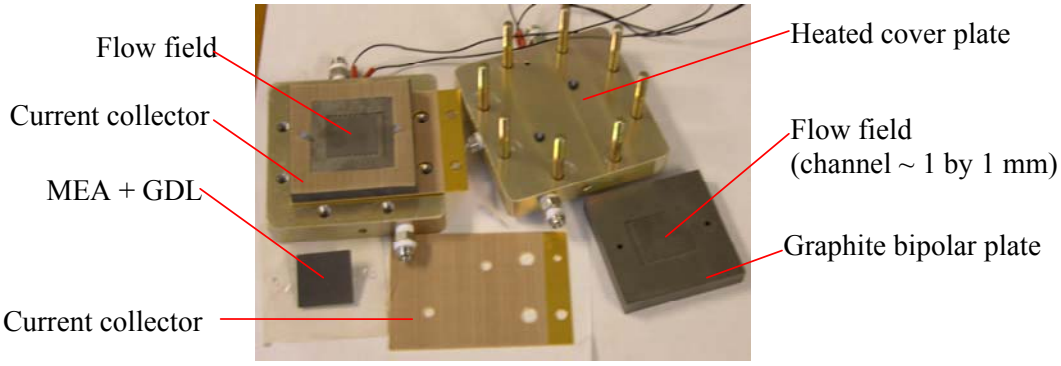

Figure 4: Commercial 10cm^2 PEMFC (by Fuel Cell Technologies),

This effort involved the following steps:

- Setting up an operational fuel cell testing facility in our laboratory: (Figure 5)
- Making membrane electrode assemblies (MEAs) with different GDL materials
- Characterization of performance in a commercial PEMFC (Figure 6)
- Direct visualization of liquid water formation and transport using an operational, transparent hydrogen-air PEMFC

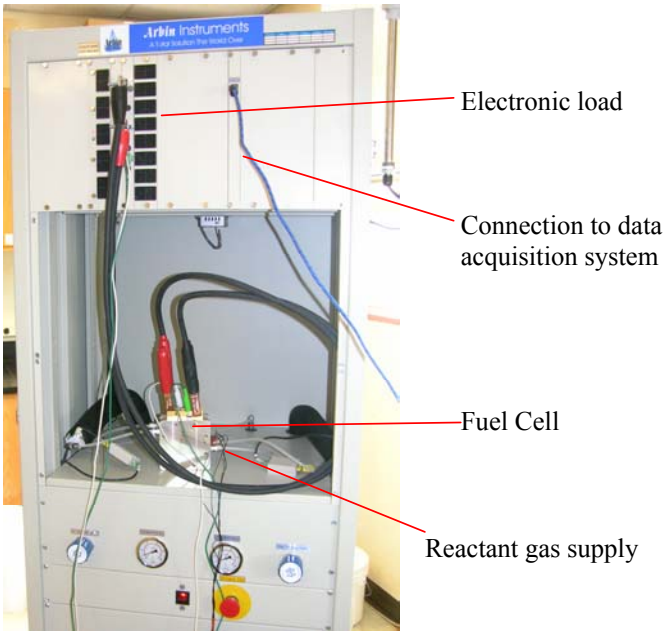

Figure 5: A 200W test station, from Arbin Instruments, is used for monitoring and control of flow, pressure, temperature, humidity and electronic load

Figure 6: Polarization curves for two GDL materials at same operating conditions

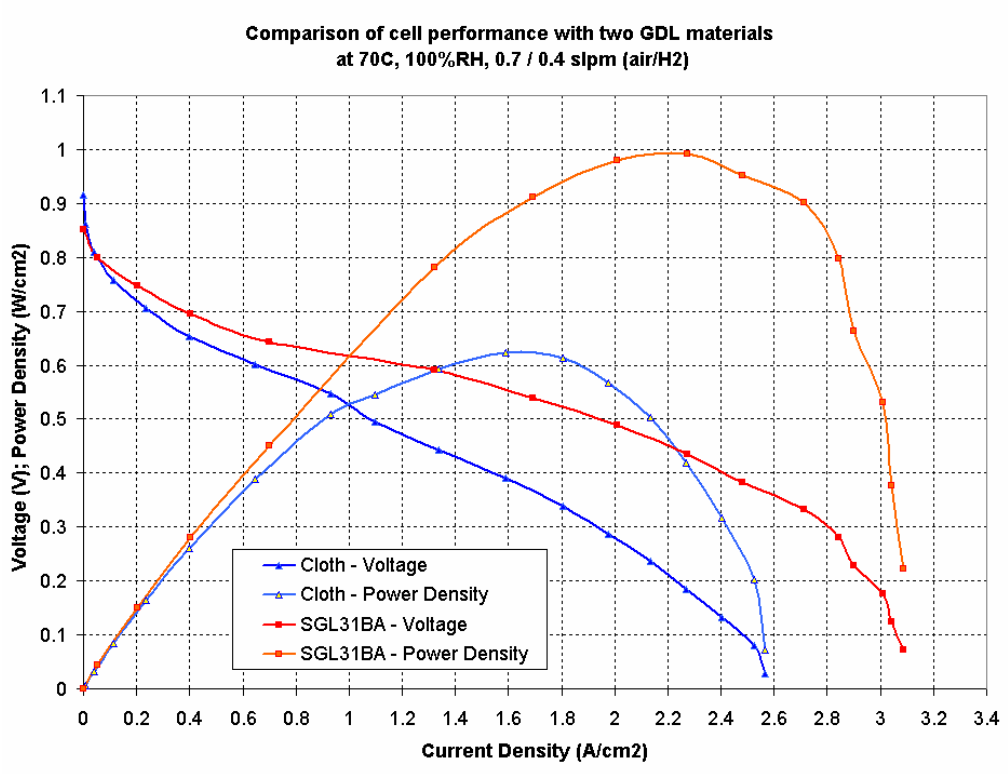

(iii) Role of Convection in Single Serpentine Flow Fields.

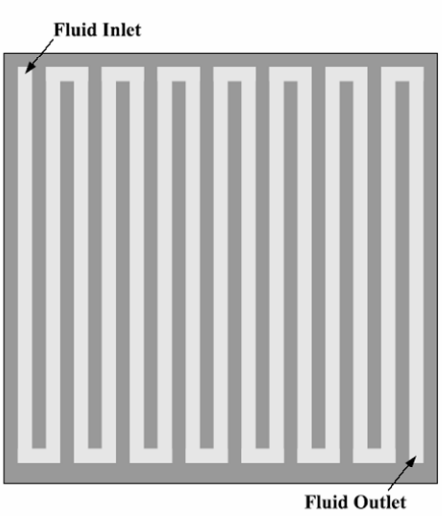

Hydrogen powered PEM fuel cells have three primary loss mechanisms: activation overpotential, ohmic overpotential, and the mass-transport limited overpotential. It is suggested that convection in the form of channel bypass can be used to increase reactant concentrations in the catalyst layer, thereby reducing the activation overpotential. Further, if convection can be made the dominant mechanism for gas transport, the diffusion-limited mass-transport overpotential can be reduced or removed. In order to determine under what conditions this can take place, an analytic model was developed for convective flow within a single serpentine channel configuration. Figure 7 shows the design of a single serpentine.

The model shows that the channel length and in-plane permeability of the gas diffusion layers are most important factors as seen from Figure 8. The analytic model was verified using a numerical code that models flow through porous media. The low relative error confirmed the assumptions made in the model.

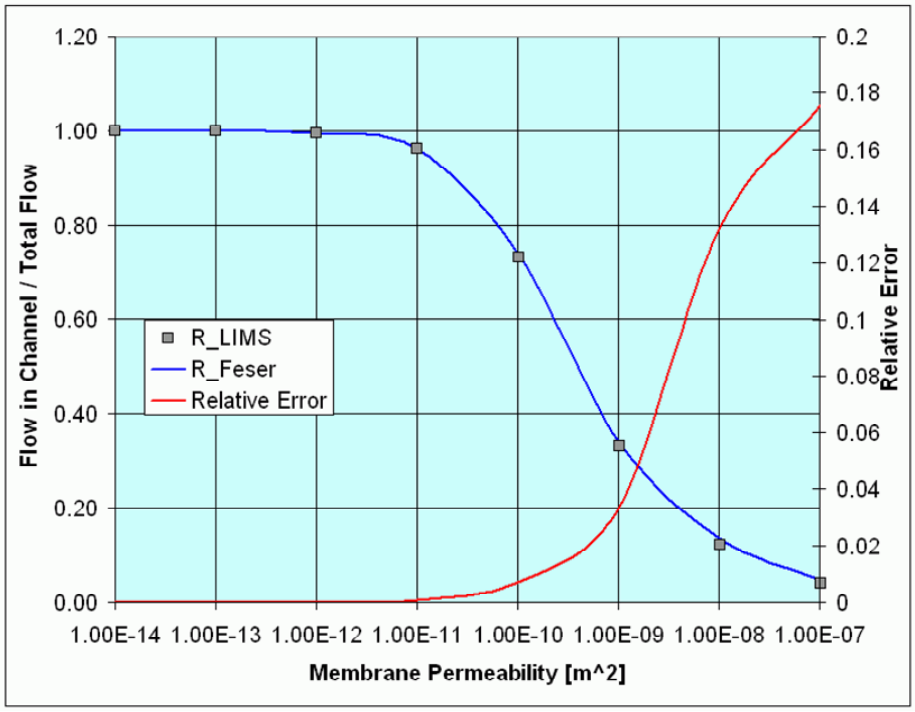

Figure 8: Convective flow as a function of GDL permeability

It has been shown that a relatively simple model can capture the physics of channel bypass in single serpentine flow field and admits a closed form solution. This model can be used to predict the relative influence of convection for a wide variety of cell design and operating parameters. It is found that the choice of GDL in-plane permeability can be a major factor in the encouragement of channel bypass driven convection. GDL thickness is found to have little impact on the relative influence of convection. It is suggested that by using rectangular cell active areas (longer channels, less passes), more channel bypass can be achieved with no additional pumping requirements.

(iv) Flow Visualization:

Particle Image Velocimetry was used to observe the velocity fields in representative test sections of an inter-digitated and a serpentine fuel cell. Using ex-situ methods, it was shown that it is possible observe secondary flows with primary to-secondary velocity ratios approaching 100-to-1. Channel bypass was observed in both configurations. Local variation in permeability appears to cause local variation in velocity fields in the channel. It was suggested to use woven type of porous media to isolate local effects of permeability. Figure 9 shows the exploded view of the cell and figure 10 shows the velocity measurements inside the cell using PIV

.

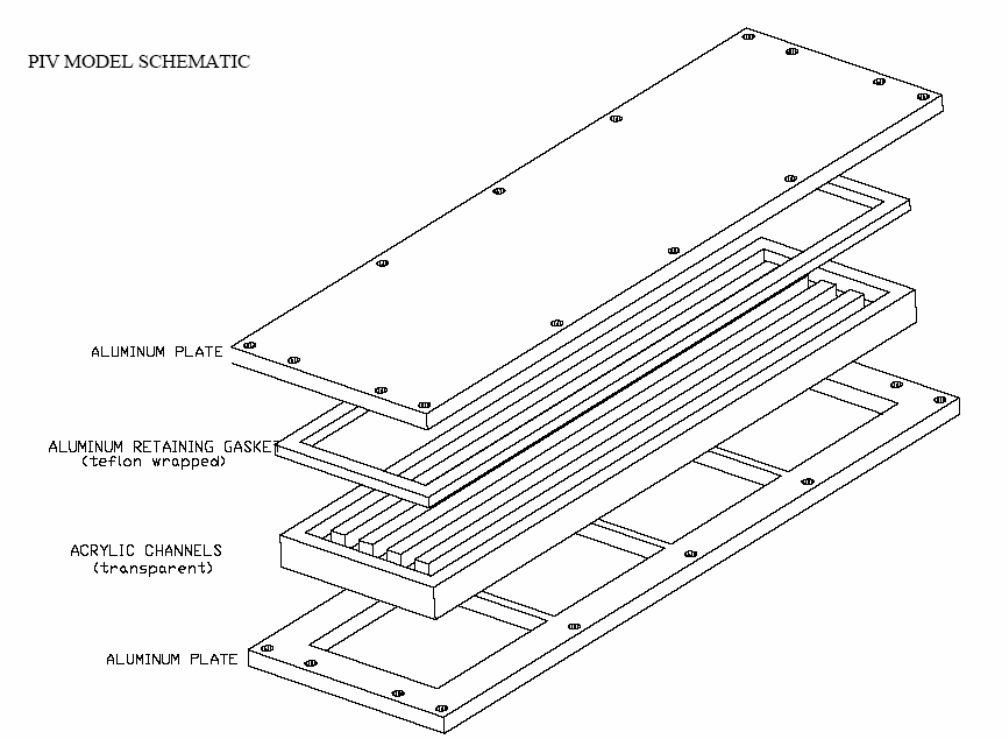

Figure 9: Exploded schematic of the flow field used in experiments

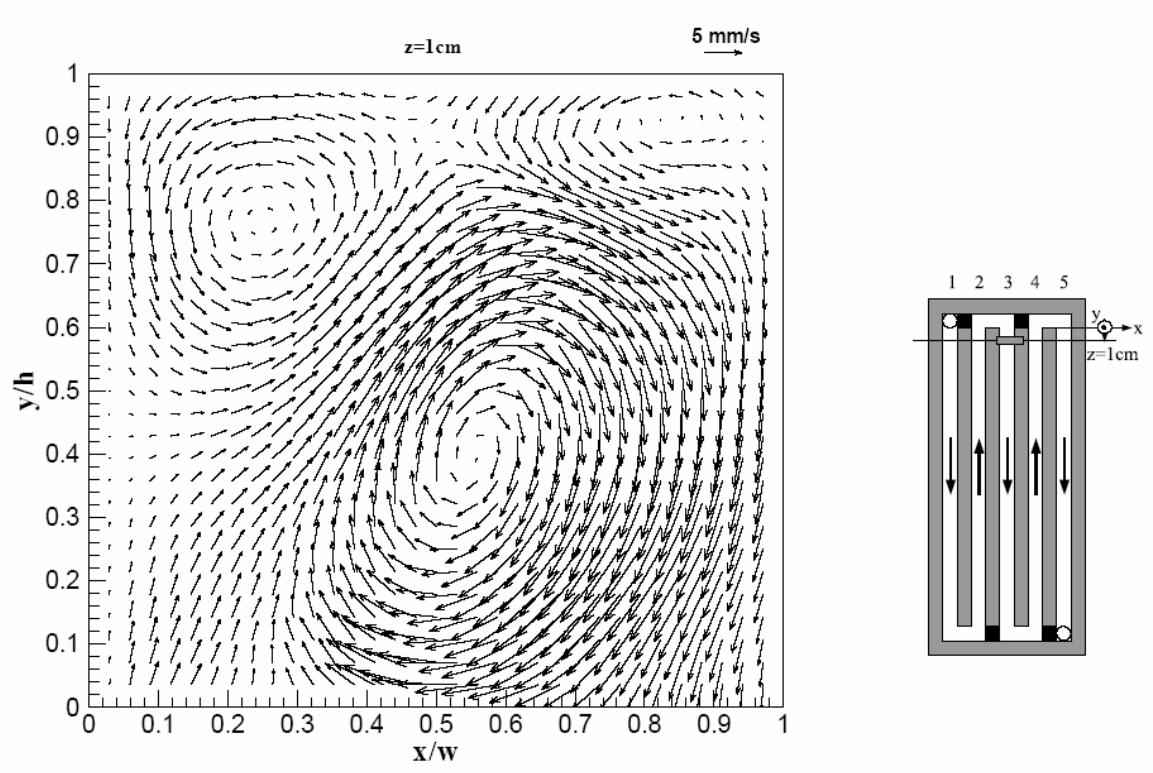

Figure 10: Time averaged velocity field at z= 1 cm (channel 3) in the serpentine flow field configuration. Significant secondary flows are present due to the proximity of the turn

Publications and Presentations:

1. Feser JP, SG Advani, and AK Prasad, "In Plane Permeability Measurements for Gas Diffusion Layers," presented at WL Gore & Associates, May 18, 2005.
2. Feser JP, AK Prasad, and SG Advani, "In Plane Permeability Measurements for Gas Diffusion Layers," in Proceedings of FUELCELL2005: Third International Conference on Fuel Cell Science, Engineering and Technology, May 23-25, 2005, Ypsilanti, MI.
3. Spernjak D, SG Advani, and AK Prasad, "Experimental Investigation of Liquid Water Formation and Transport in a Transparent Polymer Electrolyte Membrane Fuel Cell," to be presented at the Fuel Cell Seminar, November 14-18, 2005, Palm Springs, California.
4. Feser JP, SG Advani, and AK Prasad, "Particle Image Velocimetry Measurements of a Model PEMFC," in preparation, *ASME Journal of Fuel Cell Science and Technology*.
5. Feser JP, SG Advani, and AK Prasad, "In-plane Permeability Measurements of Gas Diffusion Layers," in preparation, *Journal of Power Sources*.
6. Feser JP, P. Simacek, SG Advani, and AK Prasad, "Analytic Determination of Flow Distribution in Single Serpentine Flow Fields," in preparation, *Journal of Power Sources*.

Task 8 :Durability and Failure of PEMs
PIs: Mike Santare and Anette Karlsson

Overview

Durability of the Proton Exchange Membrane (PEM) is a major technical barrier to the commercial viability of Proton Exchange Membrane Fuel Cells (PEMFC) for stationary and transportation applications. Fuel cell lifetime is currently limited by gradual degradation of both the chemical and mechanical properties of the membranes. Eventually the system fails due to a critical reduction of the voltage or mechanical damage. The objective of the research is to establish a fundamental understanding of the mechanical processes in degradation and how they influence the lifetime of PEMFCs. In the past year, we studied the effects of temperature and humidity on the mechanical properties of perfluorosulfuric acid membrane (Nafion® [1]) by using our custom-designed experimental equipments. We also developed a finite element model to investigate the in-situ hygro-thermal-mechanical stresses development in the polymer electrolyte membrane when fuel cells are under temperature and humidity changes.

Objectives

There are two objectives in this project. The first objective is to measure mechanical properties of membrane materials, including Young's modulus, proportional limit stress and dimensional change of membranes due to humidity and temperature changes. The second objective is to develop models to predict the mechanical behavior of the membranes under fuel cell service circumstances. This involves taking the results from the mechanical testing and developing those into a comprehensive constitutive model for the membranes and incorporating these into appropriate boundary value problems that approximate the loading and constraints on the material in a working fuel cell. These models can then be used to predict the hygro-thermal stresses in the polymer electrolyte membranes.

Approaches

1. Mechanical Properties of Membrane at Different Temperatures and Humidities

Tensile tests were conducted on an MTS Alliance™ RT/5 material testing system with an ESPEC custom-designed environmental chamber (Fig. 1(a)). The chamber can operate in conditions from –40˚C to 170˚C and relative humidity between 30% and 95%. Besides the sensors installed in the chamber to control the temperature and humidity of the chamber, an additional sensor is positioned close to the specimen in order to measure the temperature and humidity as close to the specimen as possible.

[1] Nafion® is a registered trademark of E.I. DuPont De Nemours & Co.

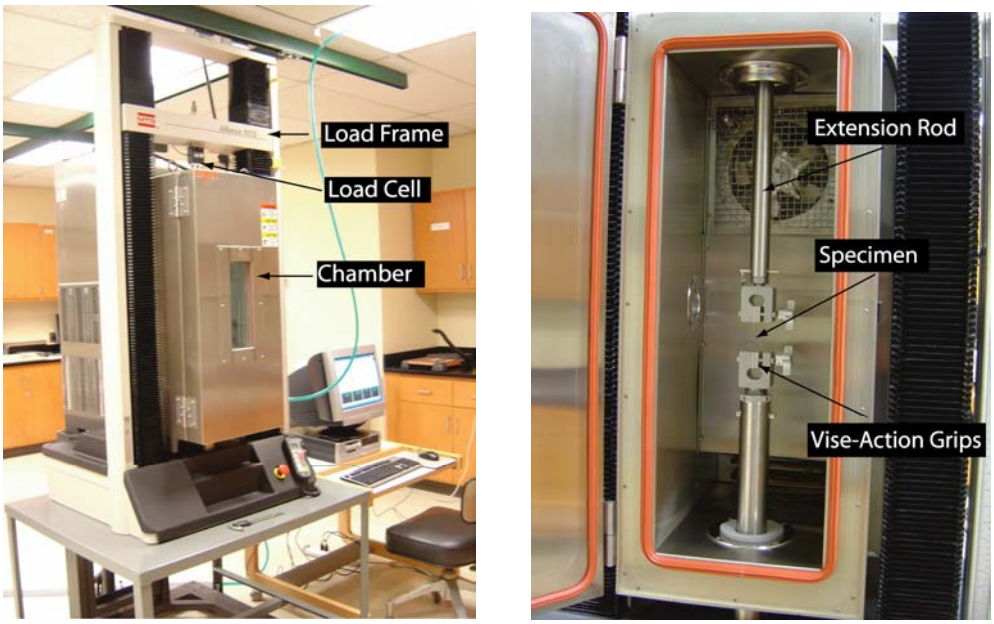

(a) (b)

Fig. 1 MTS Alliance™ RT/5 material testing system with an ESPEC custom-designed environmental chamber

In this work, membrane properties were measured at 16 different temperature and humidity combinations, i.e., at four different temperatures (25˚C, 45˚C, 65˚C, 85˚C) and four different relative humidities (30%, 50%, 70%, 90%) each. Five specimens were tested at each temperature and humidity combination. For each specimen, the thickness and width were taken as the average of three measurements distributed over the sample. The specimen was aligned with the extension rod by a pair of vise-action grips (Fig. 1(b)), and the gauge length was adjusted to 50 mm as determined by the grips separation.

2. Development of the Finite Element Model

In order to keep a tractable set of parameters, several simplifying assumptions have been made in the development of this preliminary finite element model. Whereas the actual system is three-dimensional, our model to-date is two-dimensional. An operating fuel cell has varying local conditions of temperature, humidity and power generation (and thereby heat generation) across the active area of the fuel cell. In this preliminary model, a simplified temperature and humidity profile was assumed in order to demonstrate the effects these variables can have on the stress state of the system. An illustrative temperature profile has been estimated as follows: cathode/ GDE (Gas Diffusion Electrode) and anode/GDE interface temperatures of 86 ˚C and 85 ˚C, respectively, are fixed. These values are reasonable for a fuel cell operating at 80 ˚C under typical conditions. The bipolar plate is assumed to have a constant temperature at its mid-plane, and is set to the cell operating temperature of 80 ˚C. The model then calculates the internal temperature distribution profile produced from these boundary conditions.

As a first approximation, and to reduce the computational complexity in the model, the humidity profile has been assumed uniform throughout the membrane. The

initial relative humidity of the membrane is taken as 35%, and then increased to 100% to simulate operating conditions. Both temperature and relative humidity profiles are assumed to be constant in time and there are no internal heat-generation terms. Rather, stress generation arising from humidity and temperature changes have been modeled by applying step changes in temperature and relative humidity from the initial zero-stress state of room temperature, and 35 % relative humidity. Furthermore, this initial model assumes only linear elastic response of all components, and uses the further simplifying assumption that all the materials have isotropic thermal and humidity expansion behavior (except when noted) that are uncoupled. Also, the catalyst is assumed to be integrated into the GDE instead of considering this as a separate layer. Each of these simplifying assumptions will be relaxed in future work.

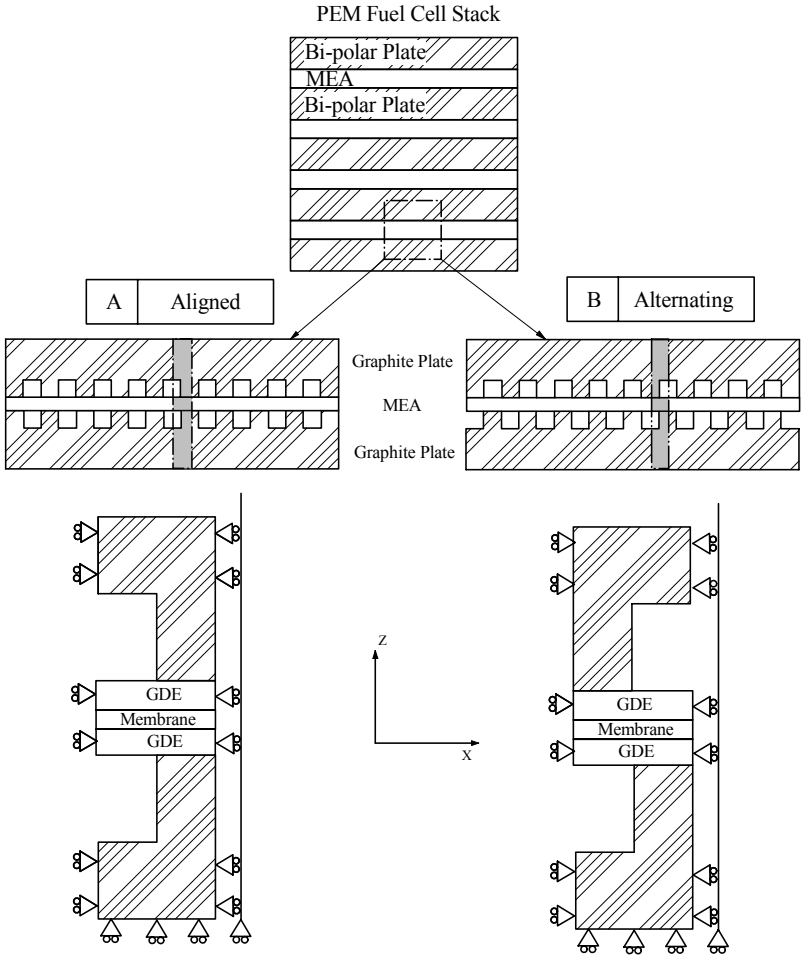

Fig. 2 Finite Element Model

Technical Accomplishments

1. Dependence of Membrane Properties on Temperature and Humidities

Effects of temperature and humidity on the mechanical properties of the membrane

The Young's modulus, proportional limit stress and elongation stress and strain are determined from each engineering stress strain plot and the average value for each of these parameters is evaluated at each temperature-humidity combination. These average values are plotted in Figs. 3 to show each parameter as a function of either temperature or relative humidity.

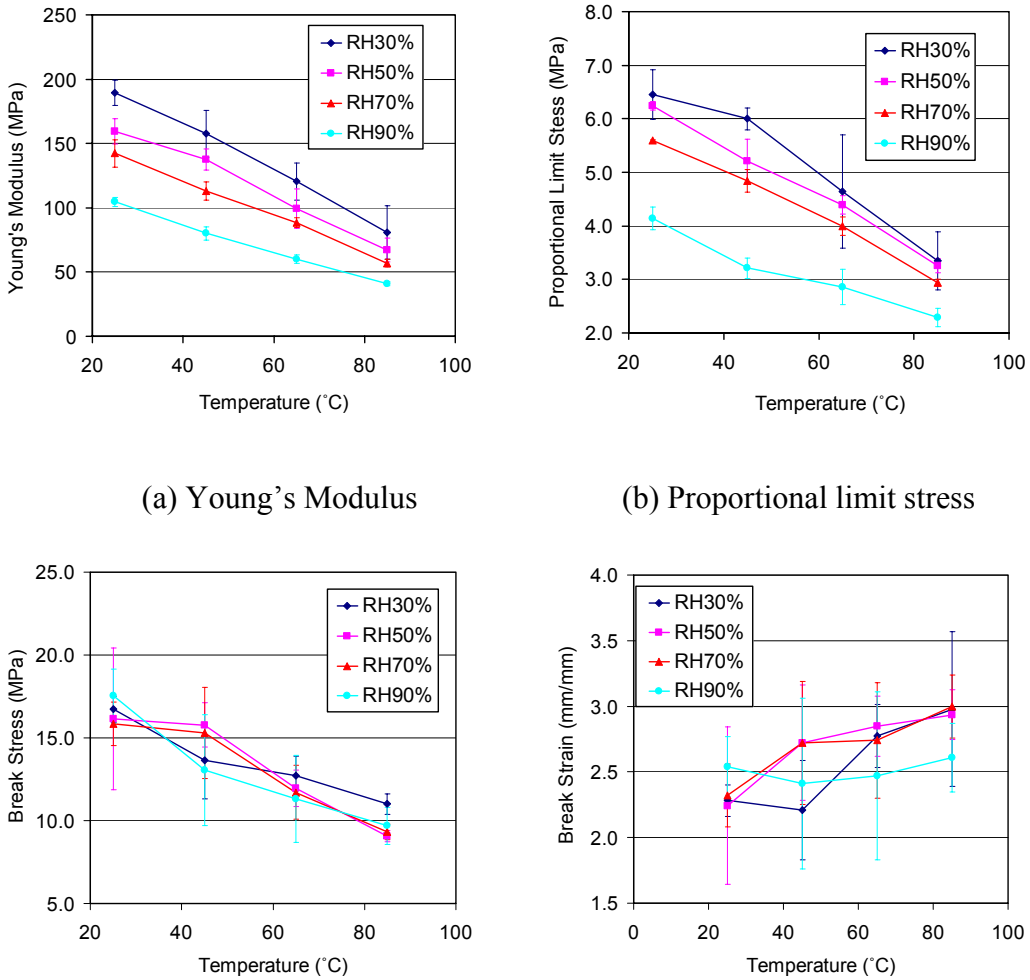

(a) Young's Modulus (b) Proportional limit stress

(c) Break stress (d) Break strain

Fig. 3 Dependence of membrane mechanical properties on temperature and humidity

The effects of temperature and humidity on the Young's modulus are shown in Fig. 3(a). The results indicate that higher temperature and relative humidity lead to lower Young's modulus. Since water has a very low glass transition temperature T_g (estimated value at -130 ºC), it acts as a very good plasticizer even in small quantity. In the presence of water, the interference between water and the chain-to-chain secondary bonding reduces the intermolecular forces. As a result, chains acquire greater mobility and free volume increases, leading to a decrease in the glass transition temperature and the strength. With the increase of the temperature, the amorphous domain with higher strength in Nafion® membrane decreases, leading to lower Young's modulus. From Fig.

3(b), we see that the proportional limit stress of Nafion® membrane also decreases as the temperature and humidity increase.

Although relative humidity apparently affects Young's modulus and the proportional limit stress, no obvious effects can be seen on break stress and elongation at break (Fig. 3(d)). However, higher temperature does lead to lower break stress and higher elongation. (Fig. 3(c)).

Swelling behaviors of the membrane at different temperatures

Dimensional changes with relative humidity at different temperatures are shown in Fig. 4. At higher relative humidity, above 70%, the coefficient increases dramatically compared with the intermediate humidity range. It is clear from Fig. 4, the swelling coefficients at higher temperature are larger than that at lower temperatures.

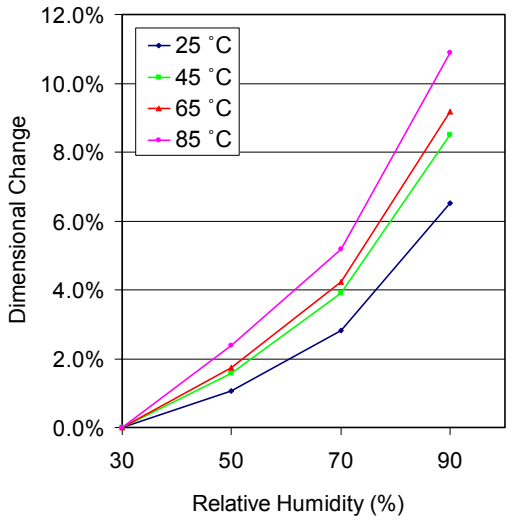

Fig. 4 Membrane dimensional changes at different temperatures

2. Stresses in the Membrane due to Hygro-Thermal Loading

Effects of plate alignments and clamping methods

In our finite element analysis, two different gas channel alignments (Aligned and Alternating, see Fig. 2) and two different clamping methods were considered. The first method is *fixed load*, in which a constant pressure (1 MPa) is applied on the surface of upper graphite plate; the second method is *fixed displacement* where the graphite plates are clamped, resulting in no net displacement in the thickness direction. These results show that the in-plane stress σ_{xx} is the dominant stress in the membrane, and the shear stress is quite small compared to in-plane and out-planes stresses. The different gas channel alignments also effect the stresses distributions. Figure 5 illustrates the stresses distributions along the upper surface of the membrane as a function of the in-plane dimension "x". It is clear that the stresses (both σ_{xx} and σ_{zz}) have the highest magnitudes in the middle of the unit cell in the alternating model, and along the edge in the aligned model. Fixed displacement clamping introduces much larger stresses in the membrane than fixed load clamping. Although the magnitudes of the differences in the stress

distributions are not large, they can induce localized bending stresses, which can contribute to failure of the system.

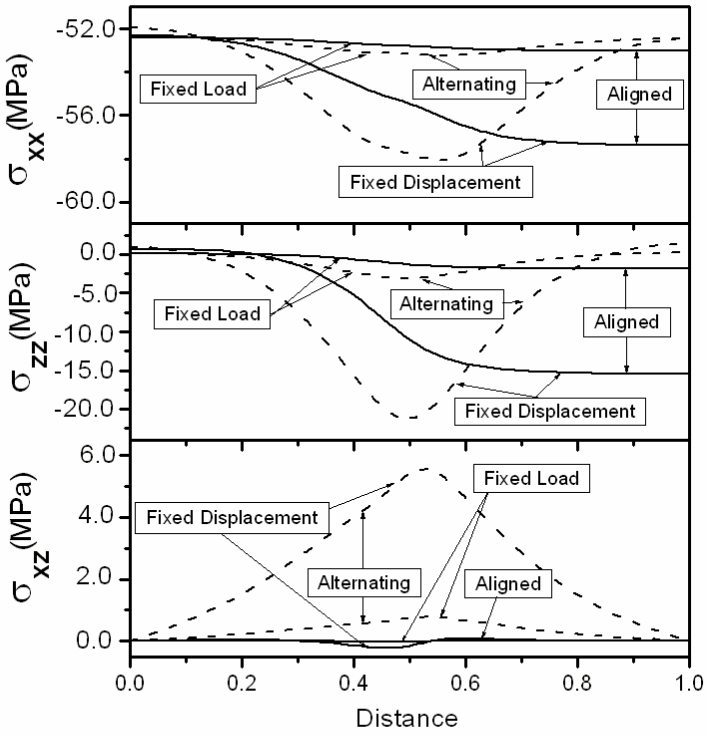

Fig. 5. A comparison of the stress distributions in the membrane along the upper surface of the membrane when using either fixed load or fixed displacement clamping methods for the two different gas channel alignments

Effect of membrane thickness

We also studied the influence of the membrane thickness on the stresses, assuming all other parameters remain unchanged. Figure 6 shows that if the plates are subjected to fixed load, changing the thickness of the membrane has a minor effect on σ_{xx}, but σ_{xz} decreases as the thickness of membrane increases in the alternating model. However, in the aligned model, σ_{xz} increases as the membrane thickness increases. If the plates are subjected to fixed displacement, all stresses increase with the increase of the membrane thickness, no mater if the gas channels are aligned or alternating.

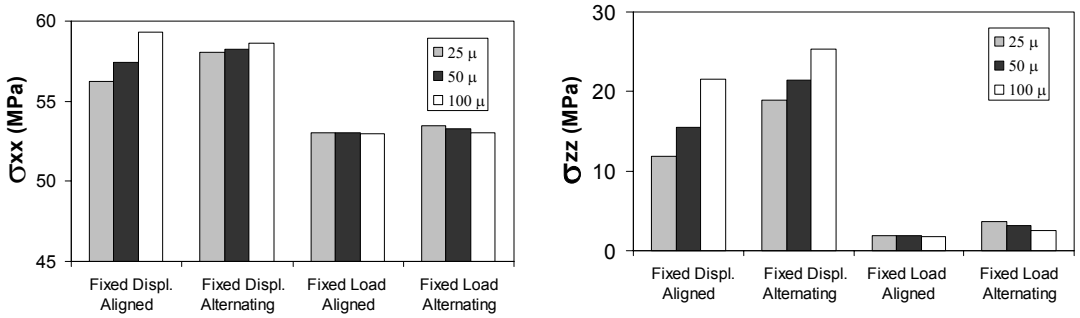

Fig. 6 The effect of thickness on the maximum in-plane stress

Investigation of Anisotropy of the membrane

Five different anisotropic cases of the membrane were investigated. Hygro-thermal stresses in the membrane (50 μm) under fixed displacement boundary condition are shown in Figures 7. The figure shows that highest stresses develop in isotropic membranes. Most significant effects on the membrane occur in the in-plane stress σ_{xx}.

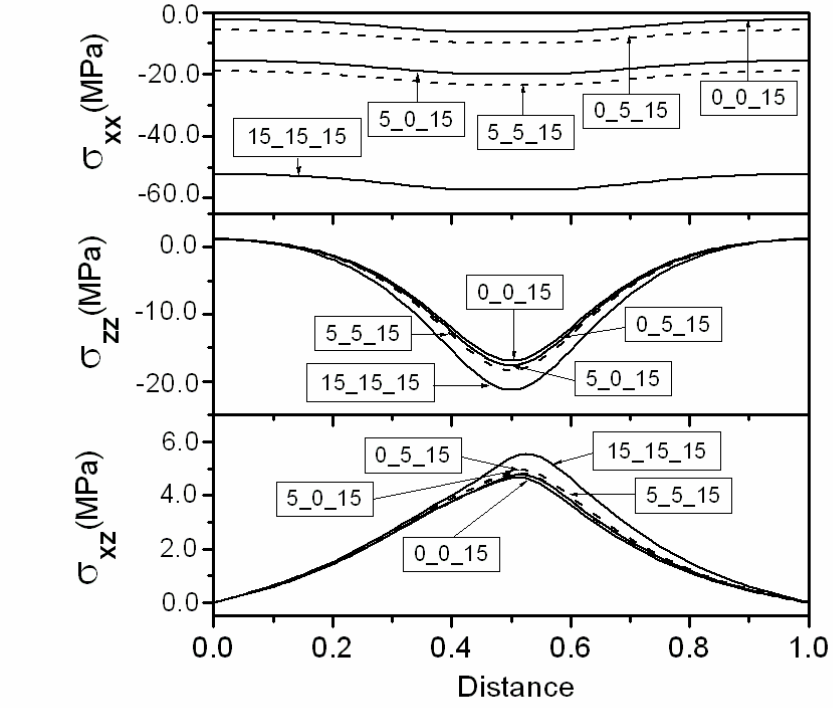

Fig. 7 The effects of anisotropy of the membrane swelling coefficient on the stress distributions in the membrane in aligned assembly

Publications and Presentations

Journals

1. Tang,Y , Santare, M.H., Karlsson, A.M., Cleghorn, S., Johnson, W.B., "Stresses in proton exchange membranes due to hydro-thermal loading". *Accepted by Journal of Fuel Cell Science and Technology.*
2. Tang,Y , Santare, Kusoglu ,A., M.H., Karlsson, A.M., Cleghorn, S., Johnson, W.B. "An Experimental investigation of humidity and temperature effects on the mechanical properties of perfluorosulfonic acid membrane". Submitted for publication.

Peer- reviewed proceedings

Tang,Y , Santare, M.H., Karlsson, A.M., Cleghorn, S., Johnson, W.B., "Stresses in proton exchange membranes due to hydration and dehydration cycles". *Proceeding of The 3rd International Conference on Fuel Cell Science, Engineering and Technology.* May 23-25, Ypsilanti, Michigan.

Presentations

1. Tang,Y , Santare, M.H., Karlsson, A.M., Cleghorn, S., Johnson, W.B., "Stresses in proton exchange membranes due to hydration and dehydration cycles". *The 3rd International Conference on Fuel Cell Science, Engineering and Technology.* May 23-25, Ypsilanti, Michigan.
2. Karlsson, A.M., Tang, Y. and Santare M.H., "Stresses in polymer electrolyte membranes due to hydro-thermal loading". 2005 ASME International Mechanical Engineering Congress and Exposition. November 5 – 11, Orlando, Florida.

Task 9: Development of Quantitative Design Tool for PEM Fuel Cells Using Lattice-Boltzmann Approach

PI: Lian-Ping Wang, Mechanical Engineering

Objectives

Computational models of increasing complexity are currently being developed to better understand issues related to the performance of PEMFC, such as pressure loss and temperature distribution in the flow channels, species transport through porous gas diffusion layers, and water management on the cathode side. A review of recent modeling efforts using traditional computational fluid dynamics (CFD) based upon macroscopic conservation equations is provided by Wang [12].

Our objective is to apply the lattice Boltzmann (LB) approach as a modeling tool for predicting fluid flows relevant to PEMFC. Unlike the traditional CFD, the LB approach is based on a kinetic formulation and could have certain advantages in handling complex flows [1,10]. While LB models capable of addressing thermal flows, flows through porous media, multiphase flows, electro-osmotic flows, and contact line, *etc.*, have been proposed in recent years, two general aspects remain to be studied before they can be applied to fuel cell modeling. The first aspect concerns the accuracy and reliability of these models for practical applications. Since these models have typically only been tested for idealized problems, their applications to PEMFC flow problems need to be critically examined and different possible LB models be compared. The second aspect concerns a variety of implementation issues when dealing with practical

applications, such as nonuniform grid, forcing implementation, boundary conditions, and porous-medium interface.

We consider these aspects using several flow problems related to PEMFC. In the following we discuss two problems that we have studied with the LB approach under the DOE support. The first is viscous flow through a section of serpentine flow channel (Fig. 1b) and we explore how to optimally and efficiently implement an LB approach. The second problem is flow through porous media for which multiple time and length scales exist.

2. Flow through a section of serpentine channel

We have investigated the pressure distribution and flow pattern in a section of serpentine channel (Fig. 1a) over a range of Reynolds numbers encountered in PEMFC. The channel has a square cross section of width W and a side length L (Fig. 1b). As a first step, we consider isothermal laminar flow and neglect the flow into the gas diffusion layer so that the back wall is treated as a no-slip wall. This similar flow was studied recently by Matharudrayya *et al.* [8] using a traditional finite-volume CFD code.

The LB equation for the distribution function (DF) f_i of the particle with velocity $\vec{e}_i$

$$f_i(\mathrm{x}+\vec{e}_i\delta t, t+\delta t) - f_i(\vec{\mathrm{x}},t) = -\frac{1}{\tau}\left[f_i(\vec{\mathrm{x}},t) - f_i^{(eq)}(\vec{\mathrm{x}},t)\right] + \psi_i(\vec{\mathrm{x}},t) \qquad (1)$$

is solved with a prescribed forcing field ψ_i designed to model the pressure difference between the inlet and the outlet, so that a periodic boundary condition can still be applied to f_i between the inlet and outlet. This minimizes the density fluctuations associated with f_i which could otherwise be significant considering the large L/W ratio here and the augmented pressure loss through the bend. The D3Q19 model [10] was used.

A nonuniform mesh along the y-direction (see Fig. 1b) is necessary for this 3D channel flow for computational efficiency. We have developed a Lagrangian interpolation method to compute DF at a grid point from the DFs on shifted grid points surrounding the grid point (Fig. 3). The method generalizes the interpolation-supplemented LB method of He et al. [7] and is easier to implement than the Taylor series expansion and least squares-based LB method of Shu et al. [11].

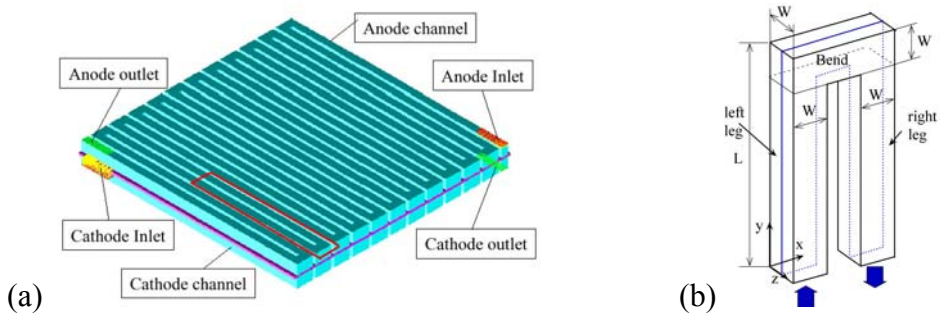

Fig. 1 (a) Sketch of serpentine flow channel in PEM fuel cell. (b) A section of the channel being modeled.

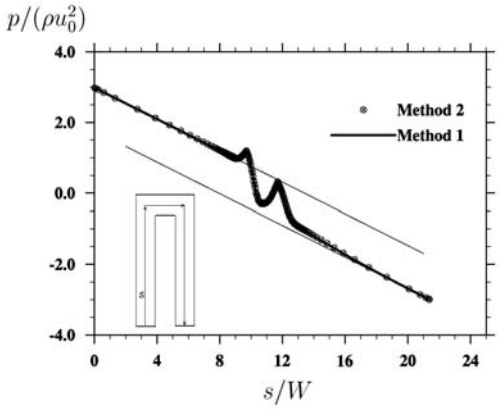

Fig. 2. The pressure as a function of the distance s along the centerline of the channel when Re=127.

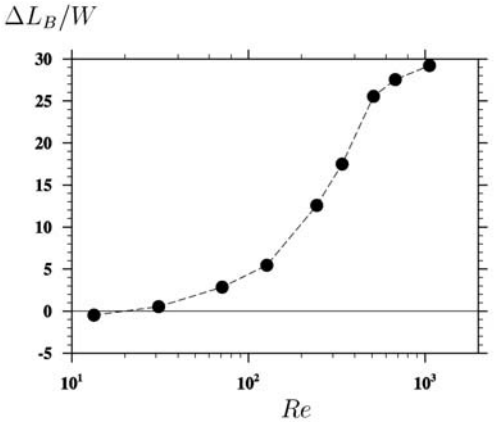

Fig. 3. The augmented loss due to the bend measured as the equivalent length of a straight channel

Fig. 2 shows a typical pressure distribution along the centerline of the channel. If the channel is made very long (*L*>>*W*), the pressure should change linearly with distance away from the bend region at both the inlet and outlet, with a same slope. This slope away from the bend can be used to define a friction factor for a straight channel (*i.e.*, $f = W\Delta p/(L\rho u_0^2/2)$). We find that this friction factor can be well modeled by the friction factor in a circular pipe (i.e., $f = 64/\mathrm{Re}$) with diameter defined as $D = 2W/\sqrt{\pi}$, namely, diameter corresponding to same cross-sectional area.

A finite jump in pressure due to the bend exists, as indicated by the vertical distance between the two thin parallel lines in Fig. 2. This is referred to as the bend pressure loss. The ratio of this jump to the slope away from the bend region defines a normalized, equivalent length for the bend pressure loss, $\Delta L_B/W$. This equivalent length is shown in Fig. 3 as a function of *Re*. Of importance is that this length increases quickly with *Re* to values comparable to the actual single-path length in a typical PEMFC, implying that the bend pressure loss must be considered in fuel cell flow modeling. The slight negative value at the lowest *Re* is due to the fact that the flow can make 180-degree turn along the inner bend at such low *Re*.

Finally, a complex flow pattern is observed at $\mathrm{Re} \approx 1000$ (Fig. 4). It appears that the flow in the bend region becomes unstable and small-scale vortices form, as seen in both *x*-y and the *z-y* planar views in Fig 4. We also find that the recovery length after the bend can be very long for high *Re*. To our knowledge, no accurate simulations for this *Re* range for a serpentine channel were made previously. Further analysis of this *Re* dependence will be reported in detail in a separate paper.

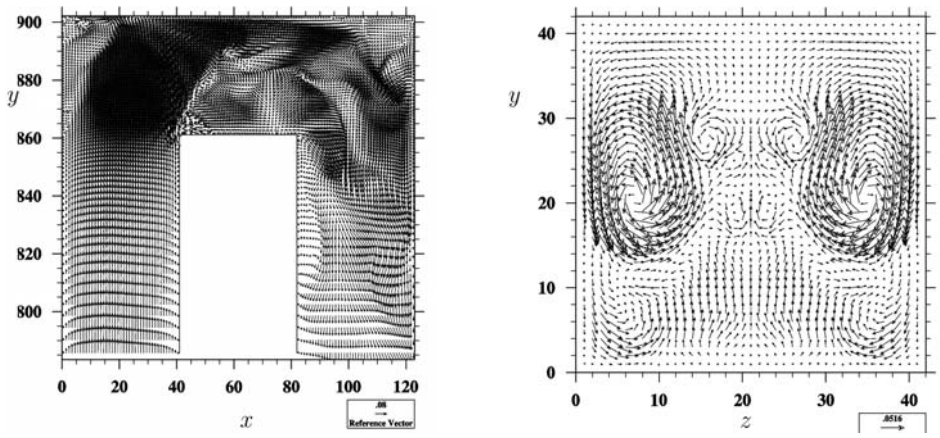

Fig. 4. *A snapshot of the quasi-steady velocity field in (a) the x-y plane through the middle of the channel and (b) the z-y plane through the middle of the bend, for Re=1059.*

3. Flow through a channel filled or partially filled with porous medium

This problem is motivated by the need to consider the interface between porous medium and clear flow channel in PEMFC modeling. We first consider flow in a 2D channel filled with porous medium of given porosity ε and permeability *K*. The macroscopic variables averaged over a representative elementary volume (REV) [9,2] are considered and they are governed by the following momentum equation incorporating a Brinkman-extended Darcy law

$$\frac{\partial \vec{u}}{\partial t} + (\vec{u}\cdot\nabla)\left(\frac{\vec{u}}{\varepsilon}\right) = -\frac{1}{\rho}\nabla(\varepsilon p) + \nu_e\nabla^2\vec{u} + \vec{F}(\vec{x},t) \quad \text{with} \quad \vec{F}(\vec{x},t) = -\frac{\varepsilon\nu}{K}\vec{u} - \frac{\varepsilon F_\varepsilon}{\sqrt{K}}|\vec{u}|\vec{u} + \varepsilon\vec{G}, \quad (2)$$

where the REV-averaged velocity $\vec{u}$ is assumed to be divergence-free, ν is fluid viscosity, ν_e is an effective viscosity, G represents the driving force for the flow. The geometric factor F_ε depends on the porosity and the microscopic configuration of porous medium (or details, see [9,2]).This approach recovers the usual Navier-Stokes equation if $\varepsilon \to 1$.

We applied the LB model derived by Guo and Zhao [2] for the above macroscopic differential equation. We first apply the LB model to a 2D channel of width *H* filled with porous medium. The flow is initially at rest and is driven by a constant pressure gradient *G* along the flow direction. In this case, the unidirectional transient flow subjected to the boundary conditions $u(y=0,t) = u(y=H,t) = 0$ can be solved analytically, giving

$$u(y,t) = \frac{GK}{\nu}\left\{1 - \frac{\cosh\left[r(y-\frac{H}{2})\right]}{\cosh\left[\frac{rH}{2}\right]}\right\} - \sum_{k=1,3,5,.....}^{\infty} \frac{4GK}{\nu}\left[\frac{(\pi k)^2}{(\pi k)^2 + (rH)^2}\right]\sin\left(\frac{\pi k y}{H}\right)\exp\left\{-\left[(\pi k)^2 + (rH)^2\right]\frac{\nu_e t}{H^2}\right\} \quad (3)$$

where $r \equiv \sqrt{\nu\varepsilon/\nu_e K}$. The analytical solution implies that there are two time scales in this problem, a diffusion time scale due to the channel walls $T_1 = H^2/(\pi^2\nu_e)$ and a diffusion time scale within the porous medium $T_2 = K/(\varepsilon\nu)$. The ratio of the two time scales T_2/T_1 is equal to T_2/T_1, which can be very small if the permeability is small. Here the Darcy number is defined as $\pi^2 Da/\varepsilon$. We find that in the implementation of the above LB scheme, it may be necessary to use a very small Darcy velocity or a large *H* to ensure that both T_1 and T_2 are much larger than one. Otherwise, an apparent slip may be present near the walls, regardless whether the midway bounce-back or the nonequilibrium extrapolation method [4] was used on the walls. This slip disappears and the analytical solution can be precisely recovered when $T_1 >> 1$ and $T_2 >> 1$. A permissible lower bound for the time scales is found to be about 50 lattice time units.

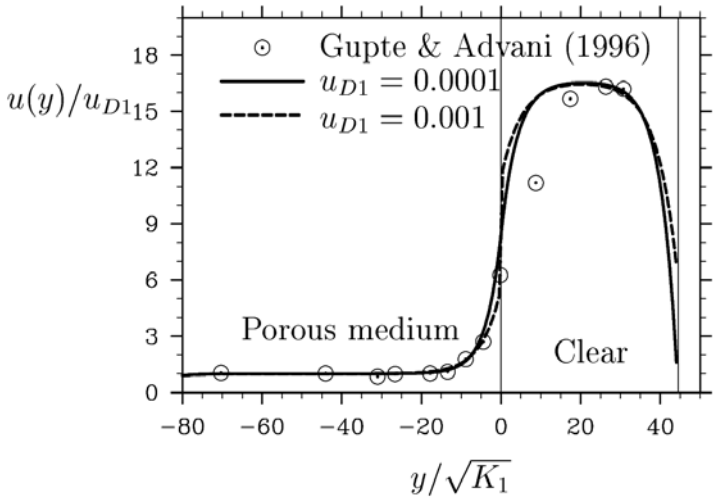

Fig. 5. Velocity profile in a channel partially filled with porous medium. Parameters are: $\varepsilon = 0.07,\ \mathrm{Re} = 0.107,\ \mathrm{K_c}/K_1 = 16.634,$ and $Da = 5.611e-5.$ *Only a part of the channel is shown. The interface is located at y=0.*

Finally, we simulated flow in a channel partially filled with porous medium so there is an interface inside the channel (Fig. 5). The velocity varies continuously across the interface only when a very small Darcy velocity was used, for the reason indicated above. Two different treatments near the interface were tested. The first method places the interface in between the lattice nodes so that only the streaming step lead to exchanges of DF between two sides of the interface. The second method treats the interface as a boundary using the nonequilibrium extrapolation method, with the density and velocity taken as the average value from the two neighboring lattice points on the two sides of the interface. The results from the two treatments are almost identical. The results are also compared with the experimental data of Gupte and Advani [6]. The discrepancy in the clear channel region near the interface may be caused by the fact that the interface is not sharply defined in the experiment. Further investigation is underway to understand the origin of this discrepancy.

Summary

Two flow problems relevant to PEMFC are simulated with the LB approach. A 3D viscous flow through a section of serpentine channel has been simulated and is shown to depend sensitively on the flow Reynolds number. The pressure distribution along both the straight portion and bend region of the channel can be quantitatively modeled. We also demonstrate that flow through a porous medium with an interface can be treated with the LB approach, provided that the existence of multiple macroscopic time scalesis taken into consideration. We have also coded and tested the LB model of Guo *et al.* [5] for thermal porous medium. Our next step would be to integrate the above components to study fluid flow in PEMFC with the flow channel and the gas diffusion layer as well as electro-osmotic effects.

We have so far focused on single-phase flows and have developed capabilities in dealing with porous medium and thermal effects. The experience will help with multiphase flow modeling in the future.

Publications and Presentations

- Lian-Ping Wang and Behnam Afsharpoya 2005, Modeling fluid flow in fuel cells using the lattice-Boltzmann approach, submitted to Applied Numerical Mathematics.

- Lian-Ping Wang and Behnam Afsharpoya, Study of viscous flow through a serpentine channel using lattice Boltzmann approach, in preparation.
- Behnam Afsharpoya, Lian-Ping Wang, and Suresh G. Advani, Modeling flow at the interface between a porous medium and a clear channel using lattice Boltzmann approach, in preparation.
- ``Modeling fluid flow and species transport in fuel cells using the lattice-Boltzmann approach", presented by Dr. Lian-Ping Wang at The 14th International Conference on Discrete Simulation of Fluid Dynamics in Complex Systems, Kyoto University, Kyoto, Japan, August 22-26, 2005.
- "Modeling fluid flow and heat transfer in PEM fuel cell using lattice-Boltzmann approach", to be presented by Dr. Behnam Afsharpoya at the 2005 Division of Fluid Dynamics meeting, American Physical Society, in Chicago.
- ``Modeling fluid transport in PEM fuel cells using the lattice-Boltzmann approach", to be presentedby Dr. Lian-Ping Wang at the 2006 Advances in Fluid Mechanics meeting organized by Wessex Institute of Technology, to be held in Skiathos, Greece, In May, 2006.

References

1. S. Chen and G. Doolen, Annu. Rev. Fluid Mech. 30 (1998) 329-364.
2. Z. Guo and T.S. Zhao, Phys. Rev. E. 66 (2002) 036304.
3. Z. Guo, C. Zheng, and B. Shi, Phys. Rev. E. 65 (2002) 046308.
4. Z. Guo, C. Zheng, and B. Shi, Chinese Physics 11 (2002) 366-374.
5. Z.L. Guo, T.S. Zhao, 2005, Progress in Computational Fluid Dynamics, 5 (2005) 110-117.
6. S.K. Gupte and S.G. Advani, Exp. in Fluids 22 (1997) 408-422.
7. X. He, L.-S. Luo, and M. Dembo, J. Comp. Phys. 129 (1996) 357-363
8. S. Maharudrayya, S. Jayanti, and A.D. Deshpande, J. Power Sources 138 (2004) 1-13.
9. P. Nithiarasu, K.N. Seetharamu, and T. Sundararajan, Int. J. Heat Mass Transfer 40 (1997) 3955-3967.
10. Y. Qian, S. Succi, and S.A. Orszag, Annu. Rev. Comput. Phys. 3 (1995) 195-242.
11. C. Shu, X.D. Niu, and Y.T. Chew, Int. J. Modern Phys. C 14 (2003) 925-944.
12. C.Y. Wang, Chem. Rev. 104 (2004) 4727-4766.